Measurement and analysis of nonhydrostatic lattice strain component in niobium to 145 GPa under various fluid pressure-transmitting media

Anil K. Singh[a)]
Materials Science Division, National Aerospace Laboratories, Bangalore 560 017, India

Takemura Kenichi
National Institute for Research in Inorganic Materials, Namiki 1-1, Tsukuba, Ibaraki 305 0044, Japan

(Received 28 March 2001; accepted for publication 27 June 2001)

The *d* spacings in niobium have been measured to 145 GPa with a diamond anvil cell using a fluid pressure-transmitting medium [methanol–ethanol–water (MEW) mixture, or helium]. The conventional geometry, wherein the primary x-ray beam passes parallel to the load axis with image plate, has been used to record the diffraction patterns. The analysis of the *d* spacings using the lattice strain equations indicates the presence of nonhydrostatic stress component (with both MEW and He pressure-transmitting media) in the pressure ranges that are well below the freezing pressure of the pressure-transmitting medium. A method to correct the measured *d* spacings for the nonhydrostatic pressure effect is suggested. This study clearly emphasizes the need to carefully analyze the data for the nonhydrostatic compression effects even if the experiments are performed with fluid pressure-transmitting medium. © *2001 American Institute of Physics.* [DOI: 10.1063/1.1397283]

I. INTRODUCTION

The diamond anvil cells (DACs) have been used extensively to record x-ray diffraction patterns from samples compressed to high pressures. These experiments give interesting information on the phase transitions and equations of state of materials over wide pressure ranges. A well-characterized stress state (ideally hydrostatic pressure) is essential for a rigorous interpretation of the diffraction data. A metal gasket[1] to contain the sample and a fluid pressure-transmitting medium is commonly used to render the stress state of the sample hydrostatic, at least up to the freezing pressure of the pressure-transmitting medium. As the pressure is raised above the freezing point[2] of the pressure-transmitting medium, the stress state of the sample begins to deviate from hydrostatic. Even at lower pressures, the stress state can become nonhydrostatic if the sample starts bridging the anvils due to excessive thinning of the gasket or due to large initial thickness of the sample. In this context, modeling[3] of the nonhydrostatic stress state and its effect on the measured lattice strains (*d* spacings) are important, as the lattice strain equations based on these models can be used to analyze the diffraction data. Equations have been derived using both the isotropic[3–9] and anisotropic[10–18] elasticity theories. The lattice strain equations based on anisotropic elasticity theory have been used by many investigators[19–35] to analyze the x-ray diffraction data under nonhydrostatic compression.

The present investigation was undertaken to look for the presence of any nonhydrostatic pressure effect in the diffraction data generated with fluid pressure-transmitting medium. We measured the *d* spacings of niobium to 145 GPa in fluid pressure medium [methanol–ethanol–water (MEW) mixture or helium]. One would invariably assume the absence of nonhydrostatic compression effects in these data, at least in the pressure ranges below the freezing pressure of the pressure-transmitting medium. However, analysis of the data using the lattice strain equations indicates the presence of a detectable nonhydrostatic stress component even in the low-pressure range. We suggest a method to correct the *d* spacings for the nonhydrostatic compression effect. Only the lower bound of the correction factor is obtained because the value of α, which defines the relative weights of Reuss and Voigt limits, is not determined. An indirect method of estimating α is discussed.

II. THEORY

A. Basic equations

The stress state of the sample compressed in an opposed-anvil setup is generally given by[3]

$$\sigma_{ij}=\sigma_P+D_{ij}, \tag{1}$$

where σ_P and D_{ij} denote the mean normal (hydrostatic) and deviatoric stress components, respectively. Assuming an axial symmetry in the stress distribution at the center of the sample, the deviatoric stress component can be expressed as follows:

$$D_{ij}=\begin{vmatrix} -t/3 & 0 & 0 \\ 0 & -t/3 & 0 \\ 0 & 0 & 2t/3 \end{vmatrix}, \tag{2}$$

where, σ_{11} and σ_{33} are the radial and axial stress components, respectively, and $t=(\sigma_{33}-\sigma_{11})$. The hydrostatic stress component is given by

$$\sigma_P=(\sigma_{11}+\sigma_{11}+\sigma_{33})/3=\sigma_{11}+t/3. \tag{3}$$

The maximum value of t is limited by the yield strength of the specimen material at a pressure σ_P. Taking the strain

a)Author to whom correspondence should be addressed; electronic mail: aksingh@css.cmmacs.ernet.in

produced by σ_P as the reference, the strain produced by the deviatoric stress component in the cubic system is given by[12,15,16]

$$[d_m(hkl)-d_P]/d_P=[a_m(hkl)-a_P]/a_P = (1-3\cos^2\psi)Q(hkl), \quad (4)$$

where, $d_m(hkl)$ denotes the measured d spacing of a set of planes (hkl) in the presence of D_{ij}, and d_P is d spacing under σ_P alone. $a_m(hkl)$ and a_P are the lattice parameters calculated from $d_m(hkl)$ and d_P, respectively. ψ denotes the angle between the diffracting plane normal and the load direction in DAC. A rearrangement of terms in Eq. (4) gives the following relation:

$$d_m(hkl)=d_P[1+(1-3\cos^2\psi)Q(hkl)]. \quad (5)$$

An equation of the same form relates $a_m(hkl)$ and a_P. If we assume that the actual stress state of the sample lies between the two extremes determined by the isostress and isostrain conditions, then

$$Q(hkl)=(t\alpha/3)\{[2G_R^X(hkl)]^{-1}-(1-\alpha^{-1})(2G_V)^{-1}\}, \quad (6)$$

where

$$[2G_R^X(hkl)]^{-1}=[S_{11}-S_{12}-3S\Gamma(hkl)], \quad (7a)$$

$$S=(S_{11}-S_{12}-S_{44}/2), \quad (7b)$$

$$\Gamma(hkl)=(h^2k^2+k^2l^2+l^2h^2)/(h^2+k^2+l^2)^2, \quad (7c)$$

and

$$(2G_V)^{-1}=5(S_{11}-S_{12})S_{44}/2[3(S_{11}-S_{12})+S_{44}]. \quad (7d)$$

The S_{ij} are the single-crystal elastic compliances at a pressure σ_P. α determines the relative weights of the isostress and isostrain conditions in an actual case, and can assume a value between 1 and 0.5. The quantity t is normally compressive and, therefore, has a negative sign. The negative sign has been included in Eq. (5) such that t is a positive number.

It is evident from Eq. (4) that the strain produced by D_{ij} vanishes at $\psi=\psi_c=\cos^{-1}(1/\sqrt{3})$, resulting in the following condition:

$$d_m(hkl)=d_P \quad (8a)$$

If we consider the fact that $(S_{11}-S_{12})$ and S_{44} are positive quantities (a requirement for the stability of the crystal lattice) and the maximum possible value of $\Gamma(hkl)$ is 1/3, then Eq. (6) suggests that $Q(hkl)$ is a positive quantity. With a positive $Q(hkl)$, the following inequalities emerge from Eq. (5):

$$d_m(hkl)>d_P \quad \text{if} \quad 0\leqslant\psi<\psi_c, \quad (8b)$$

and

$$d_m(hkl)<d_P \quad \text{if} \quad \psi_c<\psi\leqslant\pi/2. \quad (8c)$$

Equations (8a)–(8c) are also valid if $d_m(hkl)$ and d_P are replaced by $a_m(hkl)$ and a_P, respectively. In general, ψ depends on the diffraction geometry (hkl) and the mode of data recording. For the energy-dispersive mode, ψ is a constant for all (hkl). For the angle-dispersive mode, ψ depends on (hkl). For the conventional diffraction geometry with angle-dispersive mode, $\psi=(\pi/2)-\theta$. The θ range accessible in a DAC is small (usually less than ~20°). Thus, the condition given in Eq. (8c) applies to the present discussion.

B. Effect on derived quantities

The following expression is obtained from Eq. (5) for the average value of $a_m(hkl)$:

$$\langle a_m(hkl)\rangle=a_P[1+\langle(1-3\cos^2\psi)Q(hkl)\rangle]. \quad (9)$$

The angle brackets denote the average over all the observed reflections. The contribution from the nonhydrostatic compression effect to the standard deviation in $a_m(hkl)$ is given by

$$s_D=(\alpha tS)a_P[\langle\zeta^2\rangle-\langle\zeta\rangle^2]^{1/2}, \quad (10)$$

where

$$\zeta=(1-3\cos^2\psi)\Gamma(hkl). \quad (11)$$

The conventional P versus (V_m/V_0) plot constructed with the unit-cell volume measured under the nonhydrostatic compression deviates from the curve obtained under hydrostatic conditions. The deviation along the (V_m/V_0) axis is given by

$$\Delta\varepsilon_m(V)=[\langle a_m(hkl)\rangle/a_0]^3-(a_P/a_0)^3 \approx 3\langle(1-3\cos^2\psi)Q(hkl)\rangle(a_P/a_0)^3. \quad (12)$$

Since the inequality given in Eq. (8c) applies for the conventional DAC geometry, $\Delta\varepsilon_m(V)$ is a positive quantity. Thus, (V_m/V_0) at σ_{ij} is larger (and the volume strain smaller) than the value at σ_P.

C. Detection of nonhydrostatic effects

The following relation is obtained by combining Eqs. (5) and (6):

$$a_m(hkl)=M_0+M_1[3(1-3\cos^2\psi)\Gamma(hkl)], \quad (13a)$$

where

$$M_0=a_P\{1+(\alpha t/3)(1-3\cos^2\psi)[(S_{11}-S_{12}) -(1-\alpha^{-1})(2G_V)^{-1}]\}, \quad (13b)$$

$$M_1=-a_P(\alpha tS/3). \quad (13c)$$

Equation (13a) provides an extremely powerful method of detecting nonhydrostatic compression effects in the measured lattice parameters and for estimating the term (αtS). Equation (13a) suggests that the $a_m(hkl)$ versus $3(1-3\cos^2\psi)\Gamma(hkl)$ plot (termed the gamma-plot hereinafter) is a straight line if ψ is independent of (hkl), as is the case if the data are collected using the energy-dispersive mode. Even for the data obtained in the angle-dispersive mode resulting in (hkl)-dependent ψ, the term inside the curly brackets in Eq. (13b) varies within only a few percent when ψ is varied between 0° 90°. In the conventional DAC geometry, ψ varies between 90° and ~70°. For the ψ variation in this range, this term is constant within 1/10%. Thus, the gamma plots, in general, are good straight lines. A high degree of numerical precision is achieved if $(1-3\cos^2\psi)$ in

Eq. (13b) is replaced by $\langle(1-3\cos^2\psi)\rangle$, where the angle brackets denote the average taken over all the observed reflections. Further, it can be easily verified that for commonly encountered values of S_{ij} and t, $M_0 \approx a_P$. This suggests that very good estimates of (αtS) can be obtained from the following relation:

$$\alpha tS \approx -3M_1/M_0. \tag{14}$$

III. EXPERIMENTAL DETAILS

The measurements of the d spacings under pressure were performed with two different sample configurations. For measurements below 20 GPa, the sample together with a ruby chip (for pressure measurement) and pressure-transmitting medium (MEW or He) was loaded in a spring steel gasket. The estimated gasket thickness at highest pressure (20 GPa) for these experiments was ~30 μm. The estimated sample thickness at 20 GPa was ~15 μm. The sample was, therefore, not expected to come in contact with anvils up to 20 GPa. This cell assembly was used to conduct one set of experiments with MEW (series MEW-100 with a 3:1 by weight mixture of 99.9% pure niobium and platinum, 19 pressure runs in the range 0.17–18.3 GPa) and another with He (series He-500 with niobium powder, five pressure runs in the range 2.04–13.9 GPa). For measurements at higher pressure, the sample powder was filled in rhenium-gasket hole and the remaining volume was filled with pressure-transmitting medium. The sample volume in this arrangement was large, and gave strong diffraction lines. The pressure, however, was not expected to be truly hydrostatic. This cell assembly was used to carry out two sets of measurements with MEW (series MEW-300 with 1:1 niobium–silver mixture, 13 runs in the range 5.75–85.3 GPa, and series MEW-400 with niobium powder, 13 runs in the range 6.77–145 GPa). Four runs (series He-200 with 3:1 niobium–platinum mixture) with He pressure-transmitting medium were made in the range 7.64–33.46 GPa. The pressures up to 100 GPa were measured by the ruby fluorescence technique using the pressure-shift calibration[5] done under a nonhydrostatic pressure condition. The pressures above 100 GPa were estimated from the d spacings recorded from the edge of the rhenium-gasket hole, using the equation of state[36] of rhenium. The estimated errors in the pressure and d spacing measurements are discussed later in this article. The diffraction patterns were recorded with an image plate on beamline 18C of the Photon Factory, Tsukuba, Japan. The x-ray energies in the range 18–20 keV were used. In most runs, (110), (200), and (211) reflections from Nb were observed. The (220) reflection was observed in a few runs.

IV. DATA ANALYSIS AND DISCUSSION

A. General trends

Figure 1 shows the (V_m/V_0) versus pressure data from all the runs. For reference, the compression data from different sources are also plotted. Curves (1) and (3) are calculated from the Birch–Murnaghan equation of state with the bulk modulus K_0 and its pressure derivative K_0' (Table I) obtained from ultrasonic measurements[37] and theory,[38] respectively.

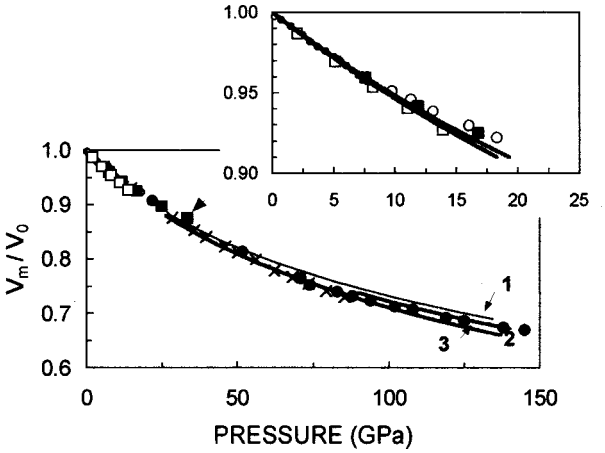

FIG. 1. Measured volume compression data of niobium. Curves (1) and (3) are calculated from the Birch–Murnaghan equation using K_0 and K_0' from ultrasonic measurement measurements (see Ref. 37) and theory (see Ref. 38) (Table I), respectively. Curve (2) shows the data obtained from shock compression experiments (see Ref. 39). The data from MEW-100, MEW-300, MEW-400, He-200, and He-500 series are shown by circles, crosses, filled circles, filled squares, and squares, respectively.

The compression data from shock wave measurements[39] are shown by curve (2). The (V/V_0) at 150 GPa calculated from the Birch–Murnaghan equation using ultrasonic data is 1.5% larger and that calculated using theoretical data 2.5% lower than the value obtained from shock wave measurements.

The volume compression data below ~8 GPa from the MEW-100 series and all the data from the He-500 series lie close (within ± 0.0005) to the compression curves (2) and (3). The first datum point at 0.17 GPa in the MEW-100 series, for some reason, shows a relatively large deviation (0.002) and is discarded in this analysis. The data points above 8 GPa of the MEW-100 series and all the data points of He-200 lie above curves (2) and (3). Most of the data points of the MEW-400 series fall above curve (3). We discuss in the foregoing sections the detailed features of these data. The data of the MEW-300 series are discussed separately in this article.

B. Detection of nonhydrostatic stress and estimation of (αtS)

The gamma plots were constructed for all the runs. The 22 runs (five from the MEW-100 series in the pressure range

TABLE I. Bulk modulus and pressure derivative of Nb.

K_0 (GPa)	K_0'	rms res.[a]	Reference
168.98(13)	4.08(1)	—	37
165	3.45	—	38
164(1)[b]	3.8(1)[b]	—	39
156(4)[c]	3.9(1)[c]	2.328[c]	Present data
142(2)[d]	4.2(1)[d]	1.578[d]	Present data
183(5)[e]	3.4(3)[e]	0.959[e]	Present data
161(1)[f]	3.2(1)[f]	0.318[f]	Present data

[a]sqrt (sum of the squares of residuals/number of data points) (GPa).
[b]From Birch–Murnaghan equation fit to shock wave data (see Ref. 39).
[c](V_m/V_0) vs P data; pressure range 0.72–145 GPa.
[d](V_P/V_0) vs P data, pressure range 0.72–145 GPa.
[e](V_m/V_0) vs P data, pressure range 0.72–50 GPa.
[f](V_P/V_0) vs P data, pressure range 0.72–50 GPa.

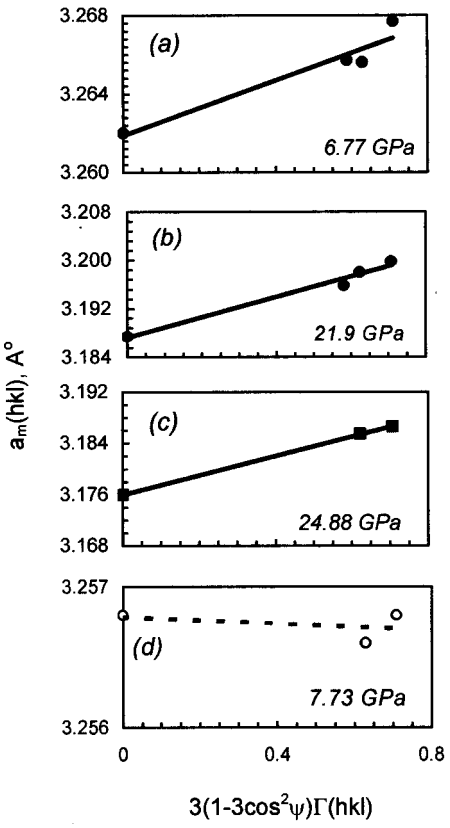

FIG. 2. A few examples of gamma plots. Symbol notations are the same as in Fig. 1.

9.76–18.33 GPa, all 13 runs from the MEW-400 series, and all four runs from He-200 series) gave straight-line plots ($R^2 \geqslant 0.83$) consistent with Eq. (13a). Figure 2(a)–2(c) show three examples of such plots. Further discussions require the knowledge of S_{ij} at high pressure. First, the C_{ij} values at a required pressure were obtained by the method suggested by Birch,[40] using the one-atmosphere C_{ij} and the pressure derivatives from ultrasonic velocity measurements.[37] The corresponding S_{ij} values are then obtained by inverting the matrix C_{ij}. The pressure dependences of $(S_{11}-S_{12})$ and S obtained by this procedure are shown in Fig. 3. It is seen that $S=-0.008\,58$ at 1 atm and -0.0062 at 150 GPa. Thus, S remains negative up to the highest pressure in these experiments. The observed positive slopes in these plots are in agreement with the sign of S. These plots suggest the presence of nonhydrostatic stress state consistent with Eqs. (1) and (2). The (αtS) values can be calculated from the slopes and intercepts of the gamma plots using Eq. (14). The estimation of t requires the knowledge of α. The choice of $\alpha = 1$ gives the lower bound of t. It is seen from Fig. 4 that the lower bounds of t range from nearly 0.2 to 3 GPa. These data indicate that $\alpha t/G(P)$ values observed in the present experiments, where $G(P)$ is the aggregate shear modulus at a pressure P, range from 0.7% to 5.6%.

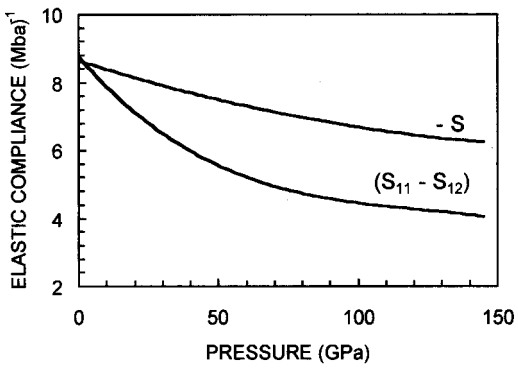

FIG. 3. The extrapolated values of S and $(S_{11}-S_{12})$ up to 145 GPa.

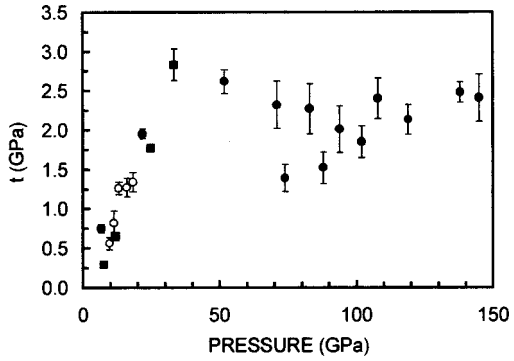

FIG. 4. The t computed with $\alpha=1$ for different runs. Symbol notations are same as in Fig. 1.

C. Hydrostatic pressure environment

The remaining 13 runs (below 8 GPa) of the MEW-100 series and all five runs of the He-500 series give plots similar to that shown in Fig. 2(d). These data sets give lines with nearly zero slopes in the gamma plots. The lattice parameters calculated from different reflections show very small scatter about the mean. This trend is expected for the cubic system under hydrostatic pressure. The measured lattice parameters $\alpha_m(hkl)$ under these conditions are independent of (hkl) and $\langle \alpha_m(hkl) \rangle$ represents a_P. For these runs, the standard deviation $s(a_m) \leqslant 0.0003$, where $s(a_m)$ denotes the standard deviation in a_m. In such cases, $s(a_m) \cong s(a_P)$ represents the intrinsic precision of measurement that can be achieved with the present setup when pressure is hydrostatic. The fact that several runs gave small $s(a_m)$ rules out the presence of any systematic error in the measurement that could possibly give rise to the observed trend in the gamma plots [Figs. 2(a)–2(c)].

D. Estimation of s_D and $s(a_P)$

The standard deviation $s(a_m)$ consists of two components. The first is the contribution from s_D [Eq. (10)] and the second from the intrinsic error in the measurement of d spacings represented by $s(a_P)$. Assuming the additivity of the variances, we get

$$s^2(a_m) = s^2(a_P) + s_D^2. \tag{15}$$

The term s_D essentially arises from the neglect of the systematic trend given by Eq. (5). The s_D values are calculated from Eq. (10) using the (αtS) values. $s(a_m)$ values are calculated from the $a_m(hkl)$ data. Equation (15) suggests

that the $s^2(a_m)$ versus s_D^2 plot should be a straight line for a constant $s(a_P)$. The intercept of the line on the $s^2(a_m)$ axis gives $s^2(a_P)$. A straight line fit through all the data gives $s(a_P)=0.0008$. This value is nearly three time larger than the value obtained for the data under an hydrostatic pressure environment. A straight line fit through the data below 20 GPa gives $s(a_P)=0.0003$, a value in good agreement with the estimate made in the preceding section. A similar analysis of the data in the pressure range 20–145 GPa gave $s(a_P)=0.0012$. The data above 20 GPa exhibit significantly larger values of $s(a_P)$ than the data in the lower pressure range. This appears to be linked to the diffraction line broadening that is found to become large above 20 GPa in the present experiments,[41] rendering the determination of the line position less precise. This analysis clearly demonstrates that the nonhydrostatic compression effect is the major source of scatter in the lattice parameters computed from different reflections.

The data from MEW-300 (shown only in Fig. 1) do not show the systematic trends discussed so far. All the data points are close to curve (3). The data points in the 5–56 GPa range show a positive deviation (average value 0.0037) from curve (3) and negative deviation (average value −0.003) in the pressure range 62–85 GPa. The slopes of the gamma plots for the data in the MEW-300 series are positive and range from 0 to 0.004. Even though the signs of the slopes are consistent with the sign of *S*, the straight-line fits are extremely poor ($0 \leqslant R^2 \leqslant 0.5$). Clearly, Eqs. (1) and (2) do not describe the stress state of the sample in these runs. The $s(a_m)$ values range between 0.002 and 0.004 and are comparable to the values in other runs (for example, in the MEW-400 series) that show good straight-line trends in the gamma plots. Because of the poor straight-line fits, correcting a_m values for the nonhydrostatic compression effect does not result in any improvement in the standard deviation and $s(a_P) \cong s(a_m)$. In view of large $s(a_m)$, the stress state cannot be considered hydrostatic. It appears that the stress distribution in the sample in the MEW-300 series was complex. It may be recalled that the sample in this series of runs was a 1:1 mixture of niobium and silver. The complex stress state of the sample may be a result of this. Further, the precision of the $d(110)$ of niobium is adversely affected by the presence of the overlapping (111) line of silver.

E. Estimates of a_P and $\Delta\varepsilon_m(V)$

The a_P values can be calculated using Eqs. (5)–(7). The $(S_{11}-S_{12})$, *S*, and $(t\alpha)$ values required in these calculations are obtained as discussed in the preceding section. However, exact calculations cannot be made, as the value of α is not known. It is seen from Eqs. (5)–(7) that $\alpha=1$ gives the lower bound of $Q(hkl)$ and also of the difference between $a_m(hkl)$ and a_P. Using this procedure, $a_P(hkl)$ values for all the reflections are calculated in each run. The calculations of $\Delta\varepsilon_m(V)$ values using these $a_P(hkl)$ values in Eq. (12) suggest that the errors in (V/V_0) introduced by the nonhydrostatic compression effect range from 0.003 to 0.022. The maximum error is found for the run at 33.46 GPa of the He-200 series. This point (marked by an arrow in Fig. 1) shows a large deviation toward higher (V/V_0) from curves (2) and (3). The corrected value falls close to these curves.

F. Equation of state

The results of fitting Birch–Murnaghan equation to the volume compression data are summarized in Table I. K_0 obtained from (V_m/V_0) is 6% lower than the estimates from theory[38] and shock wave measurements[39] and 8% lower than the value from ultrasonic measurement.[37] The value of K_0' is in good agreement with the ultrasonic and shock wave measurements. The degree of fit and the errors in K_0 and K_0' are comparable to those found in the literature. The K_0 value obtained from the (V_P/V_0) versus pressure data is nearly 10% lower and K_0' marginally higher than the corresponding values obtained from (V_m/V_0). Thus, the (V_m/V_0) data appear to yield a better value of K_0 than the (V_P/V_0) data. However, judging from the root-mean-square (rms) residual of the fit and the standard error in K_0, the (V_P/V_0) data seem to fit the Birch–Murnaghan equation significantly better than the (V_m/V_0) data.

The reason for the low value of K_0 obtained from (V_P/V_0) data can be traced to the pressure scales used in this work. As noted while reporting pressure calibration of the ruby shift,[5] the pressures obtained from the ruby-line shift are underestimated because the x-ray measured volume strains in the pressure markers were not corrected for the nonhydrostatic compression effect. Rhenium exhibits a pronounced nonhydrostatic compression effect.[8,32] This results in a gross underestimation of pressure when lines from the rhenium gasket[36] are used to estimate pressure. Consequently, both (V_m/V_0) of the niobium sample and the pressures in the present work are underestimated. This results in a partial cancellation[42] of nonhydrostatic compression effect, resulting in reasonable estimates of K_0 and K_0'. The use of the same pressure scale with (V_P/V_0) data will obviously result in a lower K_0. The nonhydrostatic compression effect on the pressure scale is presumably less pronounced in the low-pressure region. The K_0 and K_0' values obtained from compression data up to 50 GPa are also listed in Table I. The K_0 value obtained with (V_P/V_0) data is in much better agreement with the values from other sources. It should be noted that the rms residuals for Birch–Murnaghan fit are lower for (V_P/V_0) versus pressure data.

G. Further comments

The data up to ~8 GPa of the MEW-100 series and all the data of the He-500 series indicate that hydrostatic pressure can be achieved if care is taken to ensure that the sample does not bridge the anvils. The appearance of nonhydrostatic pressure above ~8 GPa in the MEW-100 series most likely results from the freezing of MEW. It is shown in a recent study[43] that hydrostatic pressure can be achieved up to at least ~50 GPa with He pressure transmitting medium by careful control of the cell assembly. The analyses of the data in other runs indicate that the pressure becomes nonhydrostatic even in the low-pressure region. Most likely, the large initial sample volume in these runs results in the sample bridging the anvils at low pressures.

The correction procedure is limited by the lack of knowledge of α. The choice of $\alpha=1$ gives the lower bound of the correction term that is required for deriving the lattice parameter corresponding to the hydrostatic component from the measured lattice parameter. Significantly lower value of root-mean-square residual of the Birch–Murnaghan fit with (V_P/V_0) data indicates that the assumption of $\alpha=1$ is valid in the present case. This conclusion is supported by the observation that a much poorer fit (rms residual=3.7) is obtained with (V_P/V_0) data calculated with $\alpha=0.5$. Based on these results, it appears possible to deduce a realistic value of α by computing (V_P/V_0) data with different values of α, and choosing the value that gives the lowest rms residual of the Birch–Murnaghan fit to the (V_P/V_0) versus pressure data.

An obvious limitation of this method is that it fails in the case of samples that exhibit isotropy in single-crystal elasticity $(S=0)$. This results in a zero slope in the gamma plot. However, as is seen from Eqs. (5)–(7), the strain from the nonhydrostatic stress component does not vanish. Further, for a given set of values of S_{ij} and αt, all $d(hkl)$ values are affected by a constant factor. An equivalent result [Eq. (10)] is that $s_D=0$. In such a case, it is not possible to detect the presence of nonhydrostatic pressure either from the gamma plots or through analysis of the standard deviations in the lattice parameters. In this context, it may be noted that the diffraction data obtained with the radial geometry[44,45] contain much more information on nonhydrostatic compression effects than the data from the conventional geometry. These data can be analyzed[16,17] to give the lattice parameters corresponding to the hydrostatic component, without requiring the value of α. The other information that can be derived from the analysis of the radial geometry data are discussed elsewhere.[16,17,32,33] The radial-geometry data can be interpreted unambiguously even when $S=0$. The lack of a straight-line trend in the gamma plot does not necessarily imply hydrostatic pressure. This may happen if the stress state of the sample is complex and does not conform to Eqs. (1) and (2). In this case, the quality of the data and the nature of the stress state have to be judged solely from the magnitude of $s(a_m)$.

The uncertainties in the estimation of S_{ij} at high pressures using Birch equations[35] are difficult to assess. The general approach used in the development of these equations is based on finite-strain theory that also forms the basis of the Birch–Murnaghan equation of state. As judged solely from the high accuracy of the Birch–Murnaghan equation in predicting the equation of state of solids, the estimates of S_{ij} at high pressures are expected to be highly reliable. In any case, the uncertainties that may exist in the estimation of S_{ij} at high pressures are unlikely to be large enough to alter the results of this analysis.

V. CONCLUSIONS

The use of fluid transmitting medium does not always result in hydrostatic pressure. The pressure may deviate from hydrostatic either when the pressure-transmitting medium solidifies or when the sample begins to bridge the anvils. The analysis presented in this article applies to the cubic system and can be used to detect the nonhydrostatic compression effects. The practice of neglecting the nonhydrostatic compression effect and taking the lattice parameter as the average of the lattice parameters calculated from the measured d spacings of the observed reflections results in overestimation of the lattice parameter and the standard deviation in the lattice parameter. The lower bound of the error in the lattice parameter arising from the neglect of the nonhydrostatic compression effect can be calculated. The contribution to the standard deviation in the lattice parameter from the nonhydrostatic compression effect can also be estimated and the contribution from the remaining sources separated. The estimation of t and a_P is limited by the lack of knowledge of α. It appears possible to obtain a reasonable estimate of α by varying α to minimize the rms residual of the Birch–Murnaghan fit to the (V_P/V_0) versus pressure data.

ACKNOWLEDGMENTS

The present experiments were performed under Proposal Nos. 97G269 and 99G204 of the Photon Factory, Tsukuba, Japan. A.K.S. thanks Ken-ichi Kondo for inviting him to the Tokyo Institute of Technology, where this work was completed. A.K.S. is a CSIR Emeritus Scientist.

[1] A. Jayaraman, Rev. Sci. Instrum. **57**, 1013 (1986).
[2] Pressure transmitting media usually exhibit a continuous increase in viscosity with increasing pressure prior to solidifying in glassy state (see Ref. 1). The onset of nonhydrostatic pressure from this source is also expected to be gradual.
[3] A. L. Ruoff, J. Appl. Phys. **46**, 1389 (1975).
[4] G. L. Kinsland and W. A. Bassett, Rev. Sci. Instrum. **47**, 130 (1976).
[5] H. K. Mao, P. M. Bell, and D. J. Steinberg, J. Appl. Phys. **49**, 3276 (1978).
[6] A. L. Ruoff, H. Xia, H. Luo, and Y. K. Vohra, Rev. Sci. Instrum. **61**, 3830 (1990).
[7] A. L. Ruoff, H. Xia, H. Luo, and Y. K. Vohra, High Press. Res. **6**, 183 (1991).
[8] R. Jeanloz, B. K. Godwal, and C. Meade, Nature (London) **349**, 687 (1991).
[9] Y. Meng, D. J. Weidner, and Y. Fei, Geophys. Res. Lett. **20**, 1147 (1993).
[10] A. K. Singh and G. C. Kennedy, J. Appl. Phys. **45**, 4686 (1974).
[11] A. K. Singh and G. C. Kennedy, J. Appl. Phys. **47**, 3337 (1976).
[12] A. K. Singh and C. Balasingh, J. Appl. Phys. **48**, 5338 (1977).
[13] A. K. Singh, J. Appl. Phys. **73**, 4278 (1993); **74**, 5920 (1993).
[14] A. K. Singh and C. Balasingh, J. Appl. Phys. **75**, 4956 (1994).
[15] T. Uchida, N. Funamori, and T. Yagi, J. Appl. Phys. **80**, 739 (1996).
[16] A. K. Singh, H. K. Mao, J. Shu, and R. J. Hemley, Phys. Rev. Lett. **80**, 2157 (1998).
[17] A. K. Singh, C. Balasingh, H. K. Mao, R. J. Hemley, and J. Shu, J. Appl. Phys. **83**, 7567 (1998).
[18] N. Funamori, M. Funamori, R. Jeanloz, and N. Hamaya, J. Appl. Phys. **82**, 142 (1997).
[19] K. Syassen and W. B. Holzapfel, Rev. Sci. Instrum. **49**, 1107 (1978).
[20] A. Onodera and A. Ohtani, J. Appl. Phys. **51**, 2581 (1980).
[21] J. C. Jamieson, Annu. Rev. Mater. Sci. **11**, 233 (1980).
[22] B. Olinger, J. Chem. Phys. **77**, 6255 (1982).
[23] S. N. Vaidya, W. A. Grosshans, and W. B. Holzapfel, High Temp.-High Press. **16**, 491 (1984).
[24] I. Videl, A. M. Redon, J. M. Leger, J. Rossat-Mignot, and O. Vogt, J. Phys. C **19**, 6297 (1986).
[25] A. Polian, J. M. Besson, M. Grimsditch, and W. A. Grosshans, Phys. Rev. B **39**, 1332 (1989).
[26] J. Leger, Phys. Chem. Miner. **17**, 161 (1990).
[27] A. K. Singh, K. Vijayan, H. Xia, Y. K. Vohra, and A. L. Ruoff, in *Recent Trends in High Pressure Research*, edited by A. K. Singh (Oxford & IBH, New Delhi, 1992), p. 782.

[28] N. Funamori, T. Yagi, and T. Uchida, J. Appl. Phys. **75**, 4327 (1994).
[29] T. S. Duffy, R. J. Hemley, and H. K. Mao, Phys. Rev. Lett. **74**, 1371 (1995).
[30] E. Wolanin, Ph. Pruzan, J. C. Chervin, B. Canny, M. Gauthier, D. Häusermann, and M. Hanfland, Phys. Rev. B **56**, 5781 (1997).
[31] R. J. Hemley, K. K. Mao, G. Shen, J. Badro, P. Gillet, M. Hanfland, and D. Häusermann, Science **276**, 1242 (1997).
[32] T. S. Duffy, G. Shen, J. Shu, H. K. Mao, R. J. Hemley, and A. K. Singh, J. Appl. Phys. **86**, 6729 (1999).
[33] T. S. Duffy, G. Shen, D. L. Heinz, J. Shu, Y. Ma, H. K. Mao, R. J. Hemley, and A. K. Singh, Phys. Rev. B **60**, 15 063 (1999).
[34] P. Grima Gallardo, J. M. Besson, J. P. Itié, M. Gauthier, M. Mezouar, S. Klotz, D. Häusermann, and M. Hanfland, Phys. Status Solidi A **180**, 427 (2000).
[35] U. Ponkratz, R. Nicula, A. Jianu, and E. Burkel, J. Phys.: Condens. Matter **12**, 8071 (2000).
[36] Y. Vohra, S. J. Duclos, and A. L. Ruoff, Phys. Rev. B **36**, 9790 (1987).
[37] K. W. Katahara, M. H. Manghanani, and E. S. Fisher, J. Appl. Phys. **47**, 434 (1976).
[38] R. Ahuja, P. Söderlind, J. Trygg, J. Melsen, J. M. Wills, B. Johansson, and O. Eriksson, Phys. Rev. Lett. **79**, 4262 (1997); private communication.
[39] R. G. McQueen, S. P. Marsh, J. W. Taylor, J. N. Fritz, and W. J. Carter, in *High-velocity Impact Phenomena*, edited by R. Kinslow (Academic, San Diego, 1970).
[40] F. Birch, J. Geophys. Res. **83**, 1257 (1978).
[41] K. Takemura, in *High Pressure Science and Technology*, edited by M. H. Manghanani, W. J. Nellis, and M. F. Nicol (Universities Press, Hyderabad, India, 2000), p. 443.
[42] This point was explicitly mentioned in the article on the pressure calibration of ruby shift (see Ref. 5).
[43] K. Takemura, J. Appl. Phys. **89**, 662 (2001).
[44] H. K. Mao and R. J. Hemley, High Press. Res. **14**, 257 (1996).
[45] H. K. Mao, J. Shu, Y. Fei, J. Hu, and R. J. Hemley, Phys. Earth Planet. Inter. **96**, 135 (1996).